Cuerda, Javier; Taskinen, Jani M.; Källman, Nicki; Grabitz, Leo; Törmä, Päivi

Observation of quantum metric and non-Hermitian Berry curvature in a plasmonic lattice

Published in:
Physical Review Research

DOI:
10.1103/PhysRevResearch.6.L022020

Published: 25/04/2024

Document Version
Publisher's PDF, also known as Version of record

Please cite the original version:
Cuerda, J., Taskinen, J. M., Källman, N., Grabitz, L., & Törmä, P. (2024). Observation of quantum metric and non-Hermitian Berry curvature in a plasmonic lattice. *Physical Review Research*, *6*(2), Article L022020. https://doi.org/10.1103/PhysRevResearch.6.L022020

PHYSICAL REVIEW RESEARCH **6**, L022020 (2024)

Letter

Observation of quantum metric and non-Hermitian Berry curvature in a plasmonic lattice

Javier Cuerda ,* Jani M. Taskinen, Nicki Källman, Leo Grabitz , and Päivi Törmä †

Department of Applied Physics, Aalto University School of Science, Aalto FI-00076, Finland

(Received 24 May 2023; accepted 25 March 2024; published 25 April 2024)

We experimentally observe the quantum geometric tensor, namely, the quantum metric and the Berry curvature, for a square lattice of radiatively coupled plasmonic nanoparticles. We observe a nonzero Berry curvature and show that it arises solely from non-Hermitian effects. The quantum metric is found to originate from a pseudospin-orbit coupling. The long-range nature of the radiative interaction renders the behavior distinct from tight-binding systems: Berry curvature and quantum metric are centered around high-symmetry lines of the Brillouin zone instead of high-symmetry points. Our results inspire pathways in the design of topological systems by tailoring losses or gain.

DOI: 10.1103/PhysRevResearch.6.L022020

Classification of matter has traditionally relied on the energy dispersion relation. Increasing attention has been paid to the structure of the eigenfunctions (Bloch functions in a crystal), characterized by the Berry curvature and the Chern number, both in electronic [1–5] and photonic [6–13] systems. Consequently, the concept of the quantum geometric tensor (QGT) [14] has gained importance. The real part of the QGT is the quantum (Fubini-Study) metric and the imaginary part gives the Berry curvature. While the Berry curvature and the Chern number have been broadly utilized, the importance of the quantum metric has only emerged recently. It has been predicted to be crucial in flat band superconductivity [15–18] and other phenomena [19,20]. The first measurements of the full QGT have been achieved recently with superconducting circuits [21], coupled qubits in diamond [22], an optical Raman lattice [23], and exciton-polariton modes in a microcavity [24,25].

Studies of topological phenomena have extended to systems with gain or loss [26–34]. Non-Hermiticity expands the classification of topological systems [35,36] and brings new concepts and applications into play [37–47]. Thus far, the QGT has been measured mostly in Hermitian systems, and only very recently the quantum metric of a non-Hermitian system has been observed [48]. To our knowledge, non-Hermitian Berry curvature has not yet been experimentally measured. In this paper, we experimentally measure the full quantum geometric tensor in a lattice of plasmonic nanoparticles and show that the quantum metric arises from (pseudo)spin-orbit coupling while the Berry curvature has a purely non-Hermitian origin.

*javier.cuerda@aalto.fi

†paivi.torma@aalto.fi

Plasmonic metal and dielectric nanoparticles coupled radiatively in two-dimensional lattices and combined with active emitters have enabled strong light-matter coupling, lasing action and Bose-Einstein condensation [49–59], and represent intriguing potential for topological photonics [60–66]. These so-called plasmonic lattices sustain unique electromagnetic modes called surface lattice resonances (SLRs) [67–69] that emerge from the long-range radiative interactions between the localized surface plasmon resonances (LSPRs) of individual nanoparticles. SLRs have highly dispersive bands with polarization-dependent properties [70,71] since nanoparticles act like small (dipole or multipole) antenna. The strength of the coupling to different directions depends on the orientation of the dipole, i.e., the polarization of the mode, see Fig. 1(a). The long-range coupling between nanoparticles makes tight binding approximations non applicable [72]. The high dissipative losses of plasmonic systems, typically considered a caveat [73,74], here turn out to be the origin of an interesting feature, namely a nonzero Berry curvature despite a trivial lattice geometry and absence of magnetic field.

We may understand the band structure of SLR modes in the two-dimensional k space with an empty lattice approximation: the diffraction orders (m, n) folded to the first Brillouin zone give the energy band dispersions of the system (see Supplemental Material, SM [75]). In the square array of Fig. 1(a), the energy of the empty lattice bands is [70,76]

$$E_{mn} = \frac{\hbar c}{n_h}\sqrt{(k_x + mG_x)^2 + (k_y + nG_y)^2}, \qquad (1)$$

where $m, n = 0, \pm 1, \pm 2 \ldots$, $G_{x,y} = 2\pi/p$, $k_{x,y}$ define the direction of the in-plane k vector, and $p = 570$ nm is the lattice period. Figure 1(b) shows the empty lattice bands along the path $\Gamma - X - M - \Gamma$ in reciprocal space. Along the trajectory Γ–M (the diagonal of the first Brillouin zone), the empty lattice mode $(0, -1)$ becomes degenerate with $(-1, 0)$; likewise (0,1) is degenerate with (1,0). For definiteness, we focus on the two transverse magnetic (TM) and transverse electric (TE) SLR bands related to empty lattice modes (0,–1) and (–1,0).

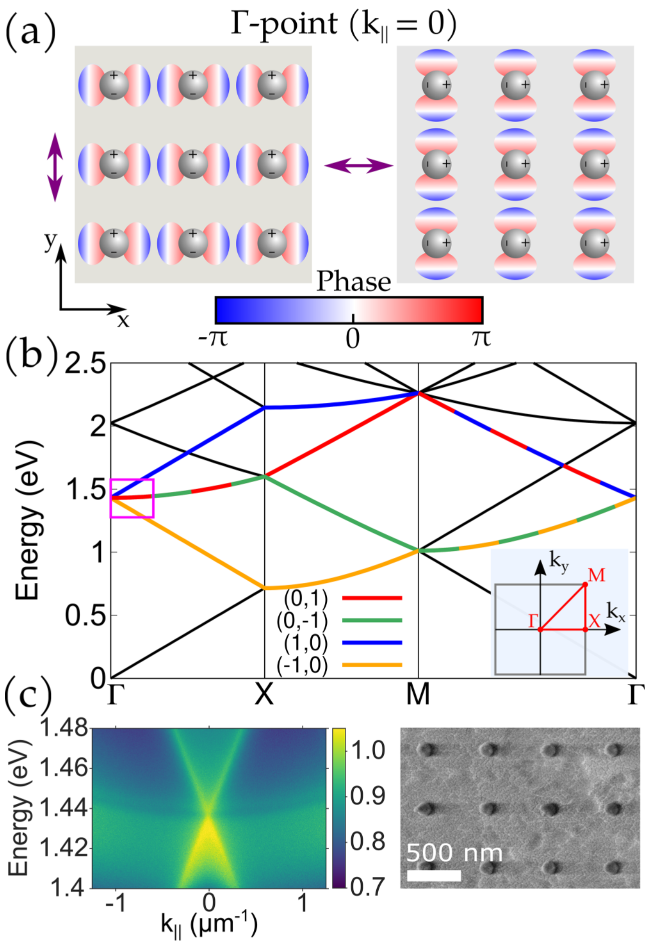

FIG. 1. (a) Schematic illustration of the SLR modes. Long-range radiative interactions (diffraction) couple the nanoparticles and create a collective mode, thus their radiation patterns acquire a phase that varies in real space depending on the lattice momentum $\mathbf{k}_{||}$ (the phase profile is only schematic, see Supplemental Material [75] for realistic simulations). On the other hand, the individual nanoparticles radiate in a highly directional and polarization-dependent manner, thus the (typically dipolar) radiation patterns are very different for TE or TM (as defined with respect to $\mathbf{k}_{||}$) incoming light polarization. At normal incidence ($\mathbf{k}_{||} = 0$), the phase difference of the in-plane electric field between different unit cells is zero and the dipolar moments oscillate all with the same phase (here denoted by having the same color at each nanoparticle). This yields two degenerate modes, identical by a $\pi/2$ rotation. (b) Band structure in the empty lattice approximation. Only the diffraction orders $(\pm 1, 0)$ and $(0, \pm 1)$ are relevant in this paper, and the rest are represented with black lines. The inset shows the trajectory $\Gamma - X - M - \Gamma$ in reciprocal space, where the Brillouin zone is delimited with grey lines. (c) Transmission measurement at the range of energies shown in the magenta square in (b) with $k_{||}$ pointing along the line Γ–X. A scanning electron micrograph of the experimental sample is provided.

The QGT is defined as

$$T_{ij}^{n} = \langle \partial_i u_{n,\mathbf{k}} | \partial_j u_{n,\mathbf{k}} \rangle - \langle \partial_i u_{n,\mathbf{k}} | u_{n,\mathbf{k}} \rangle \langle u_{n,\mathbf{k}} | \partial_j u_{n,\mathbf{k}} \rangle, \qquad (2)$$

where $\partial_i \equiv \partial_{k_i}$ with $i = x, y$. The quantum metric is $g_{ij}^n = \Re T_{ij}^n$ and the Berry curvature is $\mathfrak{B}_{ij}^n = -2\Im T_{ij}^n$. In our case, $|u_{n,\mathbf{k}}\rangle$ is the periodic part of the total Bloch function $e^{i\mathbf{k}\cdot\mathbf{r}}|u_{n,\mathbf{k}}\rangle$ of the band n. The QGT is nontrivial only in systems with multiple bands, i.e., multiple degrees of freedom ("orbitals") associated with each unit cell. In our case, these degrees of freedom are the two polarization directions of light [giving for example the TE and TM modes of Fig. 1(a)] and $|u_{n,\mathbf{k}}\rangle$ is a vector in the polarization basis. The QGT thus tells about how the polarization properties of a mode change across the Brillouin zone.

We extract the QGT from experimentally obtained lattice dispersions by adapting the methods in Refs. [24,77] to our system (see the SM [75]). Polarization-resolved transmission measurements are used to track the intensity maxima of the SLR bands [see Fig. 1(c)], from these the Stokes vector and the QGT are calculated. The samples consist of cylindrical gold nanoparticles (75-nm radius and 50-nm height) arranged in a square lattice with a periodicity of 570 nm. The QGT is related to the single-particle band structure, thus all our theoretical results and the experimental extraction scheme apply for both quantum and classical light fields. Our experiments are in the classical (many-photon) regime. We note that transmission in our case, unlike in other non-Hermitian systems [78], accurately describes the band structure and the polarization-dependent properties of the eigenmodes (see the SM [75]).

Our experiments reveal a previously unnoticed band splitting at the diagonal of the Brillouin zone, which is not predicted by the empty lattice approximation in Fig. 1(b). Figure 2(a) shows the results for $k_{||}$ pointing along the trajectory Γ–M (the diagonal), with filtering of right circularly polarized light. Interestingly, the higher (lower) energy band is TE (TM) polarized along the diagonal of the Brillouin zone, see Fig. 2(b). The similar response to left and right circular polarization filtering indicates that the chiral symmetry is not lifted in our highly symmetric square lattice. The band splitting is also observed for diagonal and antidiagonal polarizations. These polarization properties are relevant for the quantum geometric phenomena analyzed below.

The origin of the band splitting of Fig. 2(b) is explained in Figs. 1(a) and 2(c). The field profile of the lattice modes is dominated by Bloch waves of the form $\Phi(\mathbf{r}) \sim e^{i\varphi(\mathbf{r})}$ with a phase $\varphi(\mathbf{r}) = \mathbf{k} \cdot \mathbf{r}$ that has contributions from both the diffraction orders and the in-plane momentum, i.e., $\mathbf{k} = \mathbf{k}_{||} + \mathbf{G}$, where $\mathbf{G}$ is the lattice vector [70,76]. At the Γ point, the overall phase is zero, hence two degenerate modes with an in-phase radiation pattern, related by a $\pi/2$ rotation, appear [see Fig. 1(a)] and TE-TM band splitting does not take place. Along the diagonal of the Brillouin zone, the phase is nonzero giving rise to a fixed phase distribution in real space. The mode polarization is given by the dipole orientation at the single-particle level [see Fig. 2(c)], hence a given phase distribution $\varphi(\mathbf{r})$ in combination with two different polarizations (TE or TM with respect to $\mathbf{k}_{||}$) creates two fundamentally different modes and a TE-TM splitting. A thorough analysis of the band splitting using a T-matrix approach is presented in Ref. [79]. Below we provide a simplified model that relates this phenomenon with (pseudo)spin-orbit coupling.

We extract the QGT within an angular region $10^\circ < \alpha < 45^\circ$ of k space (see Fig. S4 within the SM [75]). Figure 2(d) shows that nonzero components exist for both the higher and lower energy modes in Figs. 2(a) and 2(b), with clear features

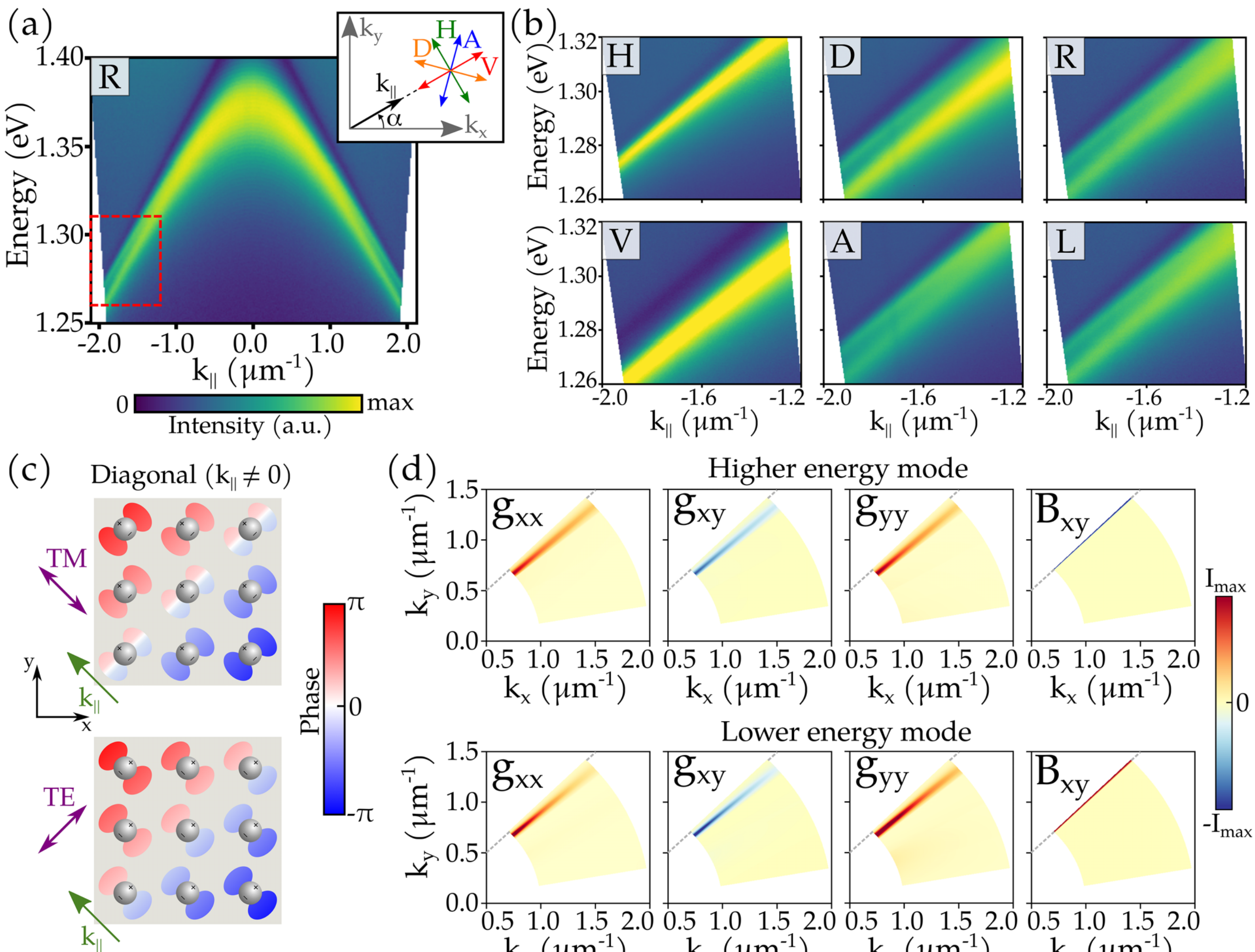

FIG. 2. (a) Transmission measurements at the diagonal of the Brillouin zone ($\alpha = 45^\circ$) for right (R) circular polarization. (b) Measurements in the red-dashed square of (a) with horizontal (H), vertical (V), diagonal (D), antidiagonal (A), right, and left (L) circular polarization filtering. (c) Explanation of TE-TM band splitting along one diagonal of the first Brillouin zone (with $\mathbf{k}_{\parallel} \neq 0$). The same phase distribution is created in real space for both TE and TM polarizations, but unlike in Fig. 1(a), the radiation patterns are different at the individual nanoparticle level, giving rise to two nondegenerate bands. The modes that participate in the band splitting are only approximately TE or TM due to the non-Hermiticity, but we name them TE and TM for practical reasons. (d) Quantum metric and Berry curvature for the higher and lower energy modes in (a) and (b), for $10^\circ < \alpha < 45^\circ$. The magnitude $I_{\max}$ of the Berry curvature is 10^{-3} times smaller than the quantum metric components. The grey-dashed line marks the diagonal of the Brillouin zone.

around the diagonal of the Brillouin zone. We find positive values for the quantum metric components g_{xx} and g_{yy}, with $g_{xx} \approx g_{yy} \approx -g_{xy}$. Remarkably, we also find a nonzero Berry curvature, which is not expected in our square lattice geometry. The Berry curvature is much smaller than the quantum metric components. Using the symmetry of the square lattice (see Fig. S1 within the SM [75] for the properties of SLR bands, and further discussion in Ref. [79]), we find that the quantum metric components are symmetric with respect to the diagonal of the Brillouin zone, and likewise the Berry curvature is antisymmetric.

We provide a simple two-band model (derived in the SM [75]) to intuitively interpret the experimental QGT results. In our model, the two bands correspond to the two polarization directions of the plasmonic-photonic modes, and the dispersion of the SLR modes is encoded in a simplified form

$$\hat{H} = \epsilon(\mathbf{k}) I_{2\times 2} + \boldsymbol{\Omega}(\mathbf{k}) \cdot \boldsymbol{\sigma}, \tag{3}$$

where

$$\epsilon(\mathbf{k}) = \frac{1}{2}(E_{-1,0}(\mathbf{k}) + E_{0,-1}(\mathbf{k})), \tag{4}$$

$$\Omega_x(\mathbf{k}) = \frac{1}{2k^2}\left(k_x^2 - k_y^2\right)(E_{0,-1}(\mathbf{k}) - E_{-1,0}(\mathbf{k})), \tag{5}$$

$$\Omega_y(\mathbf{k}) = \frac{g}{2}\sqrt{k_x^2 + k_y^2}, \tag{6}$$

and the energies $E_{-1,0}$ and $E_{0,-1}$ are defined in Eq. (1). In the most general non-Hermitian case, the Hamiltonian (3)–(6) has two sets of eigenvectors, right $|R_\pm\rangle$ and left $|L_\pm\rangle$, for each of the complex-valued eigenenergies $E_\pm(\mathbf{k})$ that define the

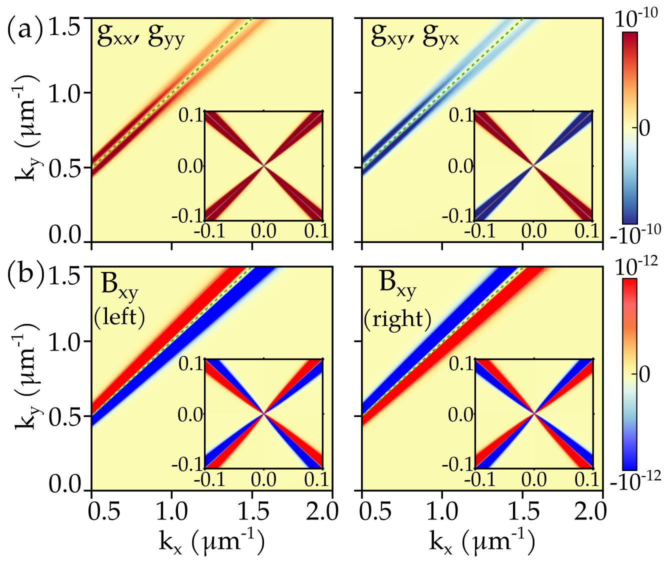

FIG. 3. QGT obtained with the two-band model. Main panels show the same area of the Brillouin zone as the experiments in Fig. 2(d), and the insets display neighboring regions to the Γ point. The green dashed line marks the diagonal of the Brillouin zone. (a) Quantum metric components. We find that $g_{xx} = g_{yy} = -g_{xy}$ and $g_{xy} = g_{yx}$. (b) Berry curvature calculated with the right and left eigenvectors of the Hamiltonian. We found that $\mathfrak{B}^n_{xy} = -\mathfrak{B}^n_{yx}$. Colorscale units are m^2.

two bands. Complete expressions of these and the QGT are found in the SM [75]. The term in Eq. (6) models the band splitting at the diagonal of the Brillouin zone, and $g = g' + ig''$ controls its size, both in the energy band structure and in the inherent losses of each mode. This minimal model is introduced to investigate degeneracy removal at the diagonal of the Brillouin zone, and it is limited to its vicinity. Nevertheless, Ref. [79] shows by detailed T-matrix calculations that the heuristic two-band model introduced here gives the same qualitative behavior as a microscopic description of the system.

The quantum metric obtained with the two-band model [see Fig. 3(a)] presents an excellent qualitative agreement with the experimental results. In both cases, the quantum metric components are nonzero around the diagonal of the Brillouin zone, and the sign of the components coincides with Fig. 2(d). The quantum metric depends essentially on the energy band splitting, and all components are zero for $g = 0$. For a typical coupling constant that fulfills $g'' \approx 10^{-2}g'$ (as in the simulations of Ref. [79]), the quantum metric is the same as in the Hermitian limit ($g'' = 0$), with negligible non-Hermitian corrections.

The Berry curvature, in contrast, strongly depends on the losses, and both the right and left forms of the Berry curvature (see the SM [75]) become zero for $g'' = 0$. This, together with our analysis in Ref. [79], proves that the Berry curvature is of non-Hermitian nature. Figure 3(b) shows the left and right Berry curvature that exhibit an excellent qualitative agreement with the experimental results, with an antisymmetric distribution at each diagonal of the Brillouin zone. The difference in magnitude between the Berry curvature and the quantum metric components is 10^{-2} in the two-band model, differing from the experimental ratio. However, microscopic simulations show good agreement with the experiments [79].

We remark that the Hamiltonian in Eq. (3) has the form of a **k**-dependent effective magnetic field $\boldsymbol{\Omega}$ coupled to a pseudospin, or a spin-orbit coupling Hamiltonian in an electronic system [80]. In our description, the polarization of light takes the role of a pseudospin, and the effective magnetic field is given by the TE/TM mode structure of a square plasmonic lattice and the band splitting at the diagonal of the Brillouin zone. The origin of the TE/TM splitting in our case is different from the one in microcavity polariton systems (see the SM [75]). Polarization-selective phenomena are observed in tight-binding systems [81], but in our lattice the splitting along the diagonal arises due to long-range radiative interactions.

The two-band model shows (see the SM [75]) that exactly at the diagonal ($\Omega_x = 0$) the quantum metric and Berry curvature always vanish, as we also see in the T-matrix simulations and experiments. Around the diagonal (in a region where $\Omega_x \sim \Omega'_y, \Omega''_y$), in the Hermitian case, a k-dependent rotation of the eigenstates in the horizontal/vertical polarization plane appears, which leads to a finite quantum metric. With losses, a net circular polarization may emerge (although not resolved by our experiments) and contribute to the Berry curvature. Intriguingly, Berry curvature can arise also due to the interplay of losses and the spin-orbit coupling, which is likely the main origin in our case.

The distribution of quantum metric and Berry curvature found here is unprecedented, following entire high-symmetry lines instead of accumulating around certain points in k space. Whereas non-Hermitian quantum metric [48] has been recently reported, our results yield, to our knowledge, the pioneering observation of Berry curvature induced by losses in optical systems.

Splittings of degenerate bands at high-symmetry points are often found in periodic systems when time-reversal symmetry is broken by (effective) magnetic field; in such cases the bandgap opening may give rise to separate bands with nonzero Chern numbers [82,83]. Here, we do not find a full bandgap in the whole Brillouin zone. Thus, time-reversal symmetry breaking by losses in our case causes nontrivial quantum geometry, but not topology. The simple two-band model we introduced can be easily adapted to other configurations, e.g., different lattice geometries [84], and will be powerful in designing topologically nontrivial structures.

Our paper lays the foundation for fertile paths of future research in long-range coupled photonic lattice systems. We anticipate that further intriguing non-Hermitian phenomena are to be found around other (than Γ) high-symmetry points [85,86], or with symmetry breaking, e.g., with multiparticle or chiral unit cells [64,66,87]. Magnetic nanoparticles may also break the time-reversal symmetry [88–90]. Finally, the above non-Hermitian effects were also found when having gain instead of losses: all these research lines may be combined with lasing or condensation phenomena. In analogy to fermionic systems [18], we expect the QGT to be relevant for bulk response in interacting, nonlinear photonic and polaritonic systems.

We acknowledge useful discussions with Mikko Rosenberg and Marek Nečada. This work was supported by the Academy of Finland under Project No. 349313, Project No. 318937 (PROFI), and the Academy of Finland Flagship Programme in Photonics Research and Innovation (PREIN) Project No. 320167, as well as by the Jane and Aatos Erkko Foundation and the Technology Industries of Finland Centennial Foundation as part of the Future Makers funding program. J.C. acknowledges former support by the Academy of Finland under Project No. 325608. J.M.T. acknowledges financial support by the Magnus Ehrnrooth Foundation. Part of the research was performed at the OtaNano Nanofab cleanroom (Micronova Nanofabrication Centre), supported by Aalto University.

[1] K. v. Klitzing, G. Dorda, and M. Pepper, New method for high-accuracy determination of the fine-structure constant based on quantized Hall resistance, Phys. Rev. Lett. **45**, 494 (1980).

[2] D. J. Thouless, M. Kohmoto, M. P. Nightingale, and M. den Nijs, Quantized Hall conductance in a two-dimensional periodic potential, Phys. Rev. Lett. **49**, 405 (1982).

[3] B. A. Bernevig and T. L. Hughes, *Topological Insulators and Topological Superconductors* (Princeton University Press, Princeton, NJ, 2013).

[4] F. D. M. Haldane, Model for a quantum Hall effect without Landau levels: Condensed-matter realization of the "parity anomaly", Phys. Rev. Lett. **61**, 2015 (1988).

[5] C. L. Kane and E. J. Mele, Z_2 Topological order and the quantum spin Hall effect, Phys. Rev. Lett. **95**, 146802 (2005).

[6] H. Price, Y. Chong, A. Khanikaev, H. Schomerus, L. J. Maczewsky, M. Kremer, M. Heinrich, A. Szameit, O. Zilberberg, Y. Yang *et al.*, Roadmap on topological photonics, J. Phys. Photon. **4**, 032501 (2022).

[7] Y. Ota, K. Takata, T. Ozawa, A. Amo, Z. Jia, B. Kante, M. Notomi, Y. Arakawa, and S. Iwamoto, Active topological photonics, Nanophotonics **9**, 547 (2020).

[8] T. Ozawa, H. M. Price, A. Amo, N. Goldman, M. Hafezi, L. Lu, M. C. Rechtsman, D. Schuster, J. Simon, O. Zilberberg, and I. Carusotto, Topological photonics, Rev. Mod. Phys. **91**, 015006 (2019).

[9] A. Khanikaev and G. Shvets, Two-dimensional topological photonics, Nat. Photon. **11**, 763 (2017).

[10] X.-C. Sun, C. He, X.-P. Liu, M.-H. Lu, S.-N. Zhu, and Y.-F. Chen, Two-dimensional topological photonic systems, Prog. Quantum. Electron. **55**, 52 (2017).

[11] L. Lu, J. Joannopoulos, and M. Soljačić, Topological photonics, Nat. Photon. **8**, 821 (2014).

[12] Y. Xu, S.-T. Wang, and L.-M. Duan, Weyl exceptional rings in a three-dimensional dissipative cold atomic gas, Phys. Rev. Lett. **118**, 045701 (2017).

[13] D. Smirnova, D. Leykam, Y. Chong, and Y. Kivshar, Nonlinear topological photonics, Appl. Phys. Rev. **7**, 021306 (2020).

[14] J. P. Provost and G. Vallee, Riemannian structure on manifolds of quantum states, Commun. Math. Phys. **76**, 289 (1980).

[15] S. Peotta and P. Törmä, Superfluidity in topologically nontrivial flat bands, Nat. Commun. **6**, 8944 (2015).

[16] L. Liang, T. I. Vanhala, S. Peotta, T. Siro, A. Harju, and P. Törmä, Band geometry, Berry curvature, and superfluid weight, Phys. Rev. B **95**, 024515 (2017).

[17] K.-E. Huhtinen, J. Herzog-Arbeitman, A. Chew, B. A. Bernevig, and P. Törmä, Revisiting flat band superconductivity: Dependence on minimal quantum metric and band touchings, Phys. Rev. B **106**, 014518 (2022).

[18] P. Törmä, S. Peotta, and B. A. Bernevig, Superconductivity, superfluidity and quantum geometry in twisted multilayer systems, Nat. Rev. Phys. **4**, 528 (2022).

[19] F. Piéchon, A. Raoux, J.-N. Fuchs, and G. Montambaux, Geometric orbital susceptibility: Quantum metric without Berry curvature, Phys. Rev. B **94**, 134423 (2016).

[20] D. Braun, G. Adesso, F. Benatti, R. Floreanini, U. Marzolino, M. W. Mitchell, and S. Pirandola, Quantum-enhanced measurements without entanglement, Rev. Mod. Phys. **90**, 035006 (2018).

[21] W. Zheng, J. Xu, Z. Ma, Y. Li, Y. Dong, Y. Zhang, X. Wang, G. Sun, P. Wu, J. Zhao *et al.*, Measuring quantum geometric tensor of non-Abelian system in superconducting circuits, Chin. Phys. Lett. **39**, 100202 (2022).

[22] M. Yu, P. Yang, M. Gong, Q. Cao, Q. Lu, H. Liu, S. Zhang, M. B. Plenio, F. Jelezko, T. Ozawa *et al.*, Experimental measurement of the quantum geometric tensor using coupled qubits in diamond, Nat. Sci. Rev. **7**, 254 (2020).

[23] C.-R. Yi, J. Yu, H. Yuan, R.-H. Jiao, Y.-M. Yang, X. Jiang, J.-Y. Zhang, S. Chen, and J.-W. Pan, Extracting the quantum geometric tensor of an optical Raman lattice by Bloch state tomography, Phys. Rev. Res. **5**, L032016 (2023).

[24] A. Gianfrate, O. Bleu, L. Dominici, V. Ardizzone, M. de Giorgi, D. Ballarini, G. Lerario, K. W. West, L. N. Pfeiffer, D. D. Solnyshkov *et al.*, Measurement of the quantum geometric tensor and of the anomalous Hall drift, Nature (London) **578**, 381 (2020).

[25] J. Ren, Q. Liao, F. Li, Y. Li, O. Bleu, G. Malpuech, J. Yao, H. Fu, and D. Solnyshkov, Nontrivial band geometry in an optically active system, Nat. Commun. **12**, 689 (2021).

[26] R. El-Ganainy, K. G. Makris, M. Khajavikhan, Z. H. Musslimani, S. Rotter, and D. N. Christodoulides, Non-Hermitian physics and PT symmetry, Nat. Phys. **14**, 11 (2018).

[27] H. Zhao, X. Qiao, T. Wu, B. Midya, S. Longhi, and L. Feng, Non-Hermitian topological light steering, Science **365**, 1163 (2019).

[28] N. Moiseyev, *Non-Hermitian Quantum Mechanics* (Cambridge University Press, Cambridge, 2011).

[29] E. J. Bergholtz, J. C. Budich, and F. K. Kunst, Exceptional topology of non-Hermitian systems, Rev. Mod. Phys. **93**, 015005 (2021).

[30] K. Ding, C. Fang, and G. Ma, Non-Hermitian topology and exceptional-point geometries, Nat. Rev. Phys. **4**, 745 (2022).

[31] N. Okuma and M. Sato, Non-Hermitian topological phenomena: A review, Annu. Rev. Condens. Matter Phys. **14**, 83 (2023).

[32] H. Nasari, G. G. Pyrialakos, D. N. Christodoulides, and M. Khajavikhan, Non-Hermitian topological photonics, Opt. Mater. Express **13**, 870 (2023).

[33] H. Liu, P. Lai, H. Wang, H. Cheng, J. Tian, and S. Chen, Topological phases and non-Hermitian topology in photonic artificial microstructures, Nanophotonics **12**, 2273 (2023).
[34] Q. Wang and Y. D. Chong, Non-Hermitian photonic lattices: tutorial, J. Opt. Soc. Am. B **40**, 1443 (2023).
[35] Z. Gong, Y. Ashida, K. Kawabata, K. Takasan, S. Higashikawa, and M. Ueda, Topological phases of non-Hermitian systems, Phys. Rev. X **8**, 031079 (2018).
[36] K. Kawabata, K. Shiozaki, M. Ueda, and M. Sato, Symmetry and topology in non-Hermitian physics, Phys. Rev. X **9**, 041015 (2019).
[37] S. Yao and Z. Wang, Edge states and topological invariants of non-Hermitian systems, Phys. Rev. Lett. **121**, 086803 (2018).
[38] J. Doppler, A. A. Mailybaev, J. Böhm, U. Kuhl, A. Girschik, F. Libisch, T. J. Milburn, P. Rabl, N. Moiseyev, and S. Rotter, Dynamically encircling an exceptional point for asymmetric mode switching, Nature (London) **537**, 76 (2016).
[39] W. Chen, Ş. K. Özdemir, G. Zhao, J. Wiersig, and L. Yang, Exceptional points enhance sensing in an optical microcavity, Nature (London) **548**, 192 (2017).
[40] J. Wiersig, Enhancing the sensitivity of frequency and energy splitting detection by using exceptional points: Application to microcavity sensors for single-particle detection, Phys. Rev. Lett. **112**, 203901 (2014).
[41] M.-A. Miri and A. Alù, Exceptional points in optics and photonics, Science **363**, eaar7709 (2019).
[42] Ş. K. özdemir, S. Rotter, and F. Nori, Parity-Time symmetry and exceptional points in photonics, Nat. Mater. **18**, 783 (2019).
[43] M. M. Denner, A. Skurativska, F. Schindler, M. H. Fischer, R. Thomale, T. Bzdušek, and T. Neupert, Exceptional topological insulators, Nat. Commun. **12**, 5681 (2021).
[44] D. D. Solnyshkov, C. Leblanc, L. Bessonart, A. Nalitov, J. Ren, Q. Liao, F. Li, and G. Malpuech, Quantum metric and wave packets at exceptional points in non-Hermitian systems, Phys. Rev. B **103**, 125302 (2021).
[45] H. Shen, B. Zhen, and L. Fu, Topological band theory for non-Hermitian Hamiltonians, Phys. Rev. Lett. **120**, 146402 (2018).
[46] D. Leykam, K. Y. Bliokh, C. Huang, Y. D. Chong, and F. Nori, Edge modes, degeneracies, and topological numbers in non-Hermitian systems, Phys. Rev. Lett. **118**, 040401 (2017).
[47] R. Su, E. Estrecho, D. Biegańska, Y. Huang, M. Wurdack, M. Pieczarka, A. G. Truscott, T. C. H. Liew, E. A. Ostrovskaya, and Q. Xiong, Direct measurement of a non-Hermitian topological invariant in a hybrid light-matter system, Sci. Adv. **7**, eabj8905 (2021).
[48] Q. Liao, C. Leblanc, J. Ren, F. Li, Y. Li, D. D. Solnyshkov, G. Malpuech, J. Yao, and H. Fu, Experimental measurement of the divergent quantum metric of an exceptional point, Phys. Rev. Lett. **127**, 107402 (2021).
[49] W. Zhou, M. Dridi, J. Y. Suh, C. H. Kim, D. T. Co, M. R. Wasielewski, G. C. Schatz, and T. W. Odom, Lasing action in strongly coupled plasmonic nanocavity arrays, Nat. Nanotechnol. **8**, 506 (2013).
[50] A. H. Schokker and A. F. Koenderink, Lasing in quasi-periodic and aperiodic plasmon lattices, Optica **3**, 686 (2016).
[51] M. De Giorgi, M. Ramezani, F. Todisco, A. Halpin, D. Caputo, A. Fieramosca, J. Gómez-Rivas, and D. Sanvitto, Interaction and coherence of a plasmon–exciton polariton condensate, ACS Photon. **5**, 3666 (2018).
[52] W. Wang, M. Ramezani, A. I. Vökeväinen, P. Tärmä, J. Gómez-Rivas, and T. W. Odom, The rich photonic world of plasmonic nanoparticle arrays, Mater. Today **21**, 303 (2018).
[53] M. Wu, S. T. Ha, S. Shendre, E. G. Durmusoglu, W.-K. Koh, D. R. Abujetas, J. A. Sánchez-Gil, R. Paniagua-Domínguez, H. V. Demir, and A. I. Kuznetsov, Room-temperature lasing in colloidal nanoplatelets via mie-resonant bound states in the continuum, Nano Lett. **20**, 6005 (2020).
[54] M. Ramezani, A. Halpin, A. I. Fernández-Domínguez, J. Feist, S. R.-K. Rodriguez, F. J. García-Vidal, and J. Gómez-Rivas, Plasmon-exciton-polariton lasing, Optica **4**, 31 (2017).
[55] T. K. Hakala, A. J. Moilanen, A. I. Väkeväinen, R. Guo, J.-P. Martikainen, K. S. Daskalakis, H. T. Rekola, A. Julku, and P. Törmä, Bose-Einstein condensation in a plasmonic lattice, Nat. Phys. **14**, 739 (2018).
[56] A. I. Väkeväinen, A. J. Moilanen, M. Nečada, T. K. Hakala, K. D. Daskalakis, and P. Törmä, Sub-picosecond thermalization dynamics in condensation of strongly coupled lattice plasmons, Nat. Commun. **11**, 3139 (2020).
[57] K. Koshelev and Y. Kivshar, Dielectric resonant metaphotonics, ACS Photon. **8**, 102 (2021).
[58] J. Guan, J.-E. Park, S. Deng, M. J. H. Tan, J. Hu, and T. W. Odom, Light-matter interactions in hybrid material metasurfaces, Chem. Rev. **122**, 15177 (2022).
[59] G. W. Castellanos, M. Ramezani, S. Murai, and J. Gómez Rivas, Non-equilibrium Bose-Einstein condensation of exciton-polaritons in silicon metasurfaces, Adv. Opt. Mater. **11**, 2202305 (2023).
[60] M. S. Rider, A. Buendía, D. R. Abujetas, P. A. Huidobro, J. A. Sánchez-Gil, and V. Giannini, Advances and prospects in topological nanoparticle photonics, ACS Photon. **9**, 1483 (2022).
[61] J. M. Taskinen, P. Kliuiev, A. J. Moilanen, and P. Törmä, Polarization and phase textures in lattice plasmon condensates, Nano Lett. **21**, 5262 (2021).
[62] S. T. Ha, Y. H. Fu, N. K. Emani, Z. Pan, R. M. Bakker, R. Paniagua-Domínguez, and A. I. Kuznetsov, Directional lasing in resonant semiconductor nanoantenna arrays, Nat. Nanotechnol. **13**, 1042 (2018).
[63] S. Murai, D. R. Abujetas, G. W. Castellanos, J. A. Sánchez-Gil, F. Zhang, and J. G. Rivas, Bound states in the continuum in the visible emerging from out-of-plane magnetic dipoles, ACS Photon. **7**, 2204 (2020).
[64] R. Heilmann, G. Salerno, J. Cuerda, T. K. Hakala, and P. Törmä, Quasi-BIC mode lasing in a quadrumer plasmonic lattice, ACS Photon. **9**, 224 (2022).
[65] W. Liu, W. Liu, L. Shi, and Y. Kivshar, Topological polarization singularities in metaphotonics, Nanophotonics **10**, 1469 (2021).
[66] G. Salerno, R. Heilmann, K. Arjas, K. Aronen, J.-P. Martikainen, and P. Törmä, Loss-driven topological transitions in lasing, Phys. Rev. Lett. **129**, 173901 (2022).
[67] V. G. Kravets, A. V. Kabashin, W. L. Barnes, and A. N. Grigorenko, Plasmonic surface lattice resonances: A review of properties and applications, Chem. Rev. **118**, 5912 (2018).
[68] B. Auguié and W. L. Barnes, Collective resonances in gold nanoparticle arrays, Phys. Rev. Lett. **101**, 143902 (2008).
[69] S. R. K. Rodriguez, A. Abass, B. Maes, O. T. A. Janssen, G. Vecchi, and J. Gómez Rivas, Coupling bright and dark plasmonic lattice resonances, Phys. Rev. X **1**, 021019 (2011).

[70] R. Guo, T. K. Hakala, and P. Törmä, Geometry dependence of surface lattice resonances in plasmonic nanoparticle arrays, Phys. Rev. B **95**, 155423 (2017).
[71] M. P. Knudson, R. Li, D. Wang, W. Wang, R. D. Schaller, and T. W. Odom, Polarization-dependent lasing behavior from low-symmetry nanocavity arrays, ACS Nano **13**, 7435 (2019).
[72] G. Weick, C. Woollacott, W. L. Barnes, O. Hess, and E. Mariani, Dirac-like plasmons in honeycomb lattices of metallic nanoparticles, Phys. Rev. Lett. **110**, 106801 (2013).
[73] A. I. Kuznetsov, A. E. Miroshnichenko, M. L. Brongersma, Y. S. Kivshar, and B. Luk'yanchuk, Optically resonant dielectric nanostructures, Science **354**, aag2472 (2016).
[74] A. Krasnok and A. Alù, Active nanophotonics, Proc. IEEE **108**, 628 (2020).
[75] See Supplemental Material at http://link.aps.org/supplemental/10.1103/PhysRevResearch.6.L022020 for further information about the empty lattice band formation, sample fabrication, finite element simulations, experimental setup and transmission measurements, derivation of the two band model, and resulting analytical expressions, origin of Berry curvature and Stokes vector analysis, comparison of transmission and eigenmode calculations, and discussion on other two band models in the available literature.
[76] R. J. Moerland, T. K. Hakala, J.-P. Martikainen, H. T. Rekola, A. I. Väkeväinen, and P. Törmä, Strong coupling between organic molecules and plasmonic nanostructures, in *Quantum Plasmonics*, edited by S. I. Bozhevolnyi, L. Martín-Moreno, and F. J. García-Vidal (Springer International Publishing, Cham, 2017), pp. 121–150.
[77] O. Bleu, D. D. Solnyshkov, and G. Malpuech, Measuring the quantum geometric tensor in two-dimensional photonic and exciton-polariton systems, Phys. Rev. B **97**, 195422 (2018).
[78] B. Zhen, C.-W. Hsu, Y. Igarashi, L. Lu, I. Kaminer, A. Pick, S.-L. Chua, J. D. Joannopoulos, and M. Soljačić, Spawning rings of exceptional points out of Dirac cones, Nature (London) **525**, 354 (2015).
[79] J. Cuerda, J. M. Taskinen, N. Källman, L. Grabitz, and P. Törmä, companion paper, Pseudospin-orbit coupling and non-Hermitian effects in the quantum geometric tensor of a plasmonic lattice, Phys. Rev. B **109**, 165439 (2024).
[80] A. Kavokin, G. Malpuech, and M. Glazov, Optical spin Hall effect, Phys. Rev. Lett. **95**, 136601 (2005).
[81] A. Poddubny, A. Miroshnichenko, A. Slobozhanyuk, and Y. Kivshar, Topological Majorana states in zigzag chains of plasmonic nanoparticles, ACS Photon. **1**, 101 (2014).
[82] S. Raghu and F. D. M. Haldane, Analogs of quantum-Hall-effect edge states in photonic crystals, Phys. Rev. A **78**, 033834 (2008).
[83] F. D. M. Haldane and S. Raghu, Possible realization of directional optical waveguides in photonic crystals with broken time-reversal symmetry, Phys. Rev. Lett. **100**, 013904 (2008).
[84] L.-H. Wu and X. Hu, Scheme for achieving a topological photonic crystal by using dielectric material, Phys. Rev. Lett. **114**, 223901 (2015).
[85] R. Guo, M. Nečada, T. K. Hakala, A. I. Väkeväinen, and P. Törmä, Lasing at *K* points of a honeycomb plasmonic lattice, Phys. Rev. Lett. **122**, 013901 (2019).
[86] X. G. Juarez, R. Li, J. Guan, T. Reese, R. D. Schaller, and T. W. Odom, M-point lasing in hexagonal and honeycomb plasmonic lattices, ACS Photon. **9**, 52 (2022).
[87] E. S. A. Goerlitzer, R. Mohammadi, S. Nechayev, K. Volk, M. Rey, P. Banzer, M. Karg, and N. Vogel, Chiral surface lattice resonances, Adv. Mater. **32**, 2001330 (2020).
[88] M. Kataja, T. K. Hakala, A. Julku, M. J. Huttunen, S. van Dijken, and P. Törmä, Surface lattice resonances and magneto-optical response in magnetic nanoparticle arrays, Nat. Commun. **6**, 7072 (2015).
[89] F. Freire-Fernández, J. Cuerda, K. S. Daskalakis, S. Perumbilavil, J.-P. Martikainen, K. Arjas, P. Törmä, and S. van Dijken, Magnetic on–off switching of a plasmonic laser, Nat. Photon. **16**, 27 (2022).
[90] N. Maccaferri, A. Gabbani, F. Pineider, T. Kaihara, T. Tapani, and P. Vavassori, Magnetoplasmonics in confined geometries: Current challenges and future opportunities, Appl. Phys. Lett. **122**, 120502 (2023).